

Ultra-stable oven designed for x-ray reflectometry and ellipsometry studies of liquid surfaces

Matt Brown, Serif Uran, and Bruce Law^{a)}

Department of Physics, Kansas State University, Manhattan, Kansas 66506-2601

Lyle Marschand and Larry Lurio

Department of Physics, Northern Illinois University, DeKalb, Illinois 60115

I. Kuzmenko and T. Gog

CMC-CAT (Sector 9), Advanced Photon Source, Argonne National Laboratory, 9700 South Cass Avenue, Illinois 60439

(Received 26 January 2004; accepted 2 May 2004; published 26 July 2004)

Stable temperature control is highly desirable for reflectivity studies of binary liquid mixtures. In this article we report on the construction of an oven that possesses good temperature stability (~ 1 mK/day) and small transverse temperature gradients (< 1 mK/cm). The oven has a horizontal geometry and can be used for either x-ray reflectometry or ellipsometry measurements from the liquid/vapor surfaces of such systems. Details of the oven design together with test results are provided. © 2004 American Institute of Physics. [DOI: 10.1063/1.1771496]

I. INTRODUCTION

The physical properties of thin liquid films are important for many applications, i.e., lubrication, painting, coating, and adhesion. Various studies of thin liquid films and interfaces over the last four decades have contributed significantly to our understanding of their structure.^{1,2} One of the techniques commonly used for structural determinations is x-ray reflectivity.^{3,4} This technique is sensitive to electron densities on thin (angstrom range) liquid films and has been extensively used to determine interfacial structures in liquids. Ellipsometry is another powerful reflectivity technique,^{5,6} used frequently in film thickness determinations. It is a simple, quick, noninvasive tabletop technique with submonolayer sensitivity to thin films. There are various advantages to being able to do both ellipsometry and x-ray reflectometry on the same sample. First, ellipsometry can be used to characterize the stability and dynamics of a system in our laboratory, the understanding of which aids in the optimization of time at a national x-ray facility where beam time is much more limited. Second, the techniques are complementary in that they are sensitive to differing length scales relevant to the systems under study, as described below. Additionally, if a model can be found that simultaneously describes the ellipsometric and x-ray reflectometry results, then this agreement provides strong evidence that the experimental results are manifestations of the physical phenomenon of interest rather than a result of some experimental artifact.

We are interested in using both ellipsometry and x-ray reflectometry to study the surfaces of liquid mixtures near a second-order phase transition, where even a small change in temperature can strongly influence both the thickness and structure of the interfacial region.⁷ The need for precise tem-

perature control makes such measurements challenging. Ideally the oven should be stable to ~ 1 mK per day with transverse temperature gradients within the oven less than 1 mK/cm. Transverse temperature gradients induce convective motion within the liquid mixture which can perturb the interfacial structure. In a binary liquid mixture the surface composition varies as a function of depth z over length scales on the order of the correlation length ξ . For critical mixtures, the correlation length $\xi \sim t^{-0.63}$ is a divergent function of the reduced temperature $t = (T - T_c)/T_c$ relative to the mixture's critical temperature, T_c , and hence the interfacial structure is a sensitive function of t . This surface variation caused by the preferential adsorption of one of the components gives rise to a local volume fraction $v(z/\xi)$ which deviates from its bulk value $v(\infty)$ depending upon the dimensionless depth z/ξ into the liquid. As mentioned above, the two experimental techniques measure different aspects of the local volume fraction because of differing sensitivities to the correlation length ξ .

In ellipsometry, the ellipticity $\bar{\rho} \equiv \text{Im}(r_p/r_s)$ at the Brewster angle is measured⁸ where r_i is the complex reflection amplitude for polarization i . For thin films ($\xi/\lambda \ll 1$), the ellipticity $\bar{\rho}$ is related to the optical dielectric profile $\varepsilon(z)$ at the surface via the Drude equation⁹

$$\bar{\rho} = \frac{\pi \sqrt{\varepsilon_1 + \varepsilon_2}}{\lambda (\varepsilon_1 - \varepsilon_2)} \int_{-\infty}^{+\infty} \frac{(\varepsilon(z) - \varepsilon_1)(\varepsilon(z) - \varepsilon_2)}{\varepsilon(z)} dz. \quad (1)$$

Here λ is the vacuum wavelength of light while $\varepsilon(z)$ varies between its value in the incident [$\varepsilon_1 = \varepsilon(-\infty)$] and reflected [$\varepsilon_2 = \varepsilon(\infty)$] media. For thick films Eq. (1) is no longer valid and the ellipticity $\bar{\rho}$ must be determined by numerically solving Maxwell's equations.^{10,11} To determine the local volume fraction $v(z)$ from $\bar{\rho}$ one must relate $\varepsilon(z)$ to $v(z)$. The usual assumption for AB mixtures is that these two quantities are related via the two-component Clausius–Mossotti equation¹²

^{a)} Author to whom correspondence should be addressed; electronic mail: bmlaw@phys.ksu.edu

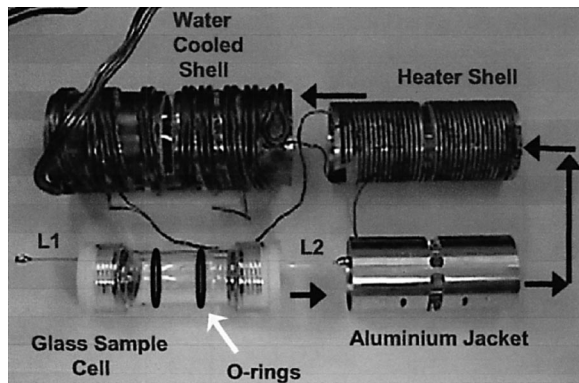


FIG. 1. Disassembled x-ray/ellipsometry oven components. The black arrows qualitatively indicate how the components are reassembled. L1 and L2 are, respectively, Luer lock fluid fill and extraction needles.

$$f(\varepsilon(z)) = v(z)f(\varepsilon_A) + (1 - v(z))f(\varepsilon_B), \quad (2)$$

where

$$f(x) = (x - 1)/(x + 2) \quad (3)$$

and ε_i is the optical dielectric constant of component i .

Analogous considerations are also applicable for x-ray reflectometry. In the first Born approximation, valid at large scattering vectors q away from the critical scattering vector, x-ray reflectivity measures^{3,4}

$$R(q) = R_F \left| \frac{1}{\rho(\infty)} \int \frac{d\rho(z)}{dz} e^{iqz} dz \right|^2 \quad (4)$$

in the absence of any surface roughness where $\rho(z)$ is the local electron density with bulk density $\rho(\infty)$, and $R_F \sim q^{-4}$ is the Fresnel reflectivity for an infinity sharp and unstructured interface. Alternatively, $R(q)$ can be determined by numerical solving Maxwell's equation where these results are valid for all q . For x-ray reflectometry, $\rho(z)$ is assumed to be related to $v(z)$ via

$$\rho(z) = v(z)\rho_A + (1 - v(z))\rho_B, \quad (5)$$

where ρ_i is the electron density for component i .

Ellipsometry and x-ray reflectometry provide rather differing experimental measures of $v(z)$ as is evident from Eqs. (1)–(5). Hence, experimental measurements using these two techniques will highly constrain the functional form $v(z)$ that can describe both data sets.

II. CONSTRUCTION DETAILS

In order to build ovens possessing good temperature stability as well as small transverse temperature gradients, the ovens need to be designed symmetrically where cylindrical symmetry is usually the most convenient. Our oven and sample cell can therefore be viewed as three concentric cylinders: an inner passive glass sample cell together with an aluminum jacket, a middle actively controlled heater shell, and an outer water cooled shell. The disassembled components are shown in Fig. 1. On assembly the aluminum jacket is held concentrically about the sample cell via appropriately placed O-rings. The aluminum jacket, heater shell, and water shell are then held concentrically with respect to each other via nylon tipped set screws where a ~ 1 mm air gap sepa-

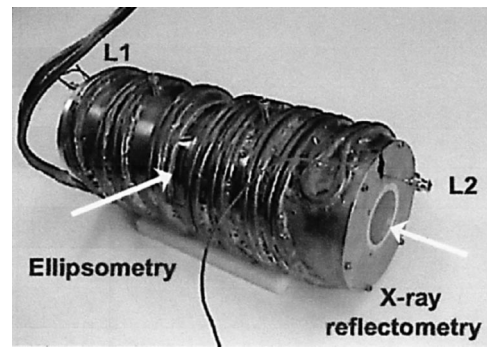


FIG. 2. Assembled x-ray/ellipsometry oven where the windows for x-ray and ellipsometry measurements are indicated by the white arrows.

rates the jacket, heater shell, and water shell, thus providing a weak thermal link. During assembly it is very important to maintain the cylindrical symmetry to high accuracy in order to minimize thermal instabilities and thermal gradients. The fully assembled oven of total length 10 in. and outer cylindrical diameter 4 in. is shown in Fig. 2. X-ray scattering and reflectivity measurements are made along the cylinder axis while ellipsometry measurements can be conducted through the semi-cylindrical glass windows. The Luer lock needle L1 has two purposes: (i) it enables one to replace air with helium gas, thus minimizing the build up of ozone gas, and (ii) it acts as a fill port for the critical liquid mixture. Luer lock needle L2, which dips into the liquid sample trough, acted as a sample extraction needle. By over-pressurizing the oven via L1 using helium gas, a liquid sample can readily be extracted out of L2 for further testing.

There are a number of important construction details that require more extensive description. The outer water cooled shell is “double wrapped” with copper tubing so that water enters and exits the tubing from the same side, as shown in Fig. 1. In this configuration the double wrapping ensures that the colder inlet water compensates for the hotter outlet water. “Single wrapping” of the copper tubing, with the water inlet and outlet on opposite ends of the cooler shell would, by contrast, induce a temperature gradient along the length of the cooler shell. In normal operation the cooler shell was maintained at ~ 3 °C below the temperature of the heater shell using a water bath possessing a stability of ~ 0.01 °C.

The heater shell (Fig. 1) is constructed from aluminum and has very uniform machined grooves along its length. Laminated heating wire, possessing a resistance of 1.6 Ω /ft (Pelican Wire Co.), is permanently embedded in the grooves using the epoxy Wakefield Delta Bond 155. To minimize any temperature gradients it is important to ensure that the resistance of the heating wire is identical on the left and right halves of the heater oven before permanently embedding the wire in the grooves. Note that the use of heating wire provides more uniform heating than, for example, two Minco heaters placed symmetrically on the left and right halves of the oven because Minco heaters are only specified to be identical to within $\pm 10\%$. For optimal control and measurement of the temperature, the temperature sensing element must exhibit a large reproducible change in some physical property per °C, in the temperature range of interest. Most of the

critical mixtures that we study possess a critical temperature somewhere between 20 °C and 60 °C. In this range, thermistors possess an excellent sensitivity where the resistance decreases with increasing temperature and the temperature can readily be measured to sub-mK resolution. We use Yellow Springs Instrument 44 034 thermistors as the sensing and measuring element where the nominal resistance at 25 °C is 5 k Ω . They are extremely useful for measuring relative changes in the temperature in the vicinity of the critical temperature. Although these thermistors only have a nominal accuracy of 0.1 °C, thermistors possessing identical serial numbers exhibit much better thermal characteristics than this. From a dozen thermistors (of identical serial number), one can usually find three or four matched pairs which exhibit identical readings in the vicinity of T_c to within a few mK. Such matched pairs are useful for accurately measuring temperature gradients as described later. One of these thermistors, immersed in thermally conducting paste (Omegatherm 201); within a 1.25 in. deep hole inside the heater shell, serves as the sensing element for a Lakeshore DRC-91C temperature controller.

Critical mixtures are very sensitive to the presence of impurities. Impurities on the order of a few percent can change the critical temperature by many degrees.¹³ This change in T_c is not problematic, provided that T_c is stable and does not drift significantly with time. If the critical mixture reacts with any components of the sample cell, T_c is likely to drift with time. From past experience we only trust a few materials to be in direct physical contact with our critical mixtures, specifically, certain glasses (pyrex, fused and crystalline quartz), teflon, teflon-encapsulated O-rings, and chemically resistant stainless steel (type 316). As a point of reference, for certain glass encapsulated critical mixtures such as isobutyric acid+water, T_c might drift at most a few mK/month. Our sample cell has therefore been constructed primarily from these materials where we have taken particular care about which materials come into direct contact with the critical mixture.

The glass sample cell [GC in Fig. 3(a)] is constructed from two threaded glass connectors (Ace Glass, Cat. No. 7644-25) where two teflon bushings (Ace Glass, Cat. No. 7506-35) hold two type 316 stainless steel end caps (SSC) in place with the sealing between the stainless steel and glass being accomplished using chemically resistant Kalrez O-rings.¹⁴ The internal construction of the sample cell is shown in Fig. 3(a) together with the fill (L1) and extraction needles (L2). The end caps possess kapton windows through which x rays can pass. A glass sample trough is situated inside a larger overflow teflon trough. Within the glass trough a glass slide is positioned approximately 0.5 mm below the top edge of the glass trough using a U-shaped glass support [Fig. 3(b)]. With the critical mixture heated well into the one-phase region (to prevent phase separation during filling), sufficient liquid is placed into the glass trough such that it overflows this container and flows into the larger teflon trough. In this manner the liquid/vapor surface is configured to sit above the glass trough where the glass slide helps to minimize vibrational disturbances of this liquid/vapor surface. It is important to prealign the glass trough horizontally

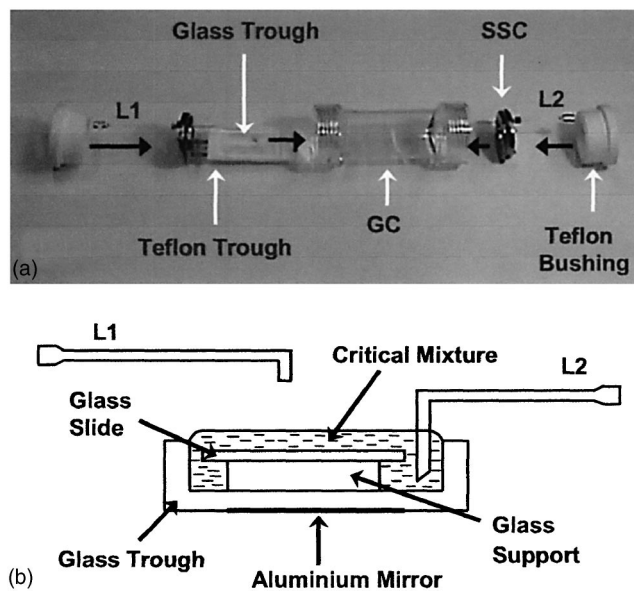


FIG. 3. (a) Disassembled sample cell showing the glass and teflon troughs, fill (L1) and extraction (L2) Luer lock needles, glass cell (GC), stainless steel cap (SSC), and teflon bushings. The black arrows qualitatively indicate how the components are reassembled. (b) Schematic cross-section of critical mixture in the glass trough.

because the x rays are incident on the liquid/vapor surface near grazing incidence. To assist with this horizontal alignment the glass trough possesses an aluminum mirror on its bottom surface; horizontality is attained when a vertical laser beam is reflected back on itself from the mirrored bottom surface. The glass trough is readily cleaned using a glass etch solution (5% HF, 35% HNO₃, and 60% H₂O by volume), then rinsed well in ultra-clean water before drying. As ellipsometry is sensitive to any optical birefringence, it is important to anneal any glass windows through which the ellipsometric beam may pass. These components should also be held in a manner which minimizes mechanical stress to the glass.

Transverse temperature gradients along the axis of the sample cell are measured using matched thermistors which are placed in good thermal contact with the stainless steel end caps using thermal paste. The temperature is measured to sub-mK accuracy via a simple voltage measurement series circuit (Fig. 4) incorporating an ultra-stable voltage source, LM399. The precision voltage reference LM399 is temperature compensated with less than 2 ppm drift per °C.¹⁵ The Vishay Dale precision reference resistance R_0 (~ 250 k Ω) with a temperature coefficient of ± 50 ppm/°C limits the current through the thermistor to ~ 20 μ A to minimize any Joule heating of the thermistor, which may perturb the temperature measurement itself.

III. RESULTS AND DISCUSSION

Figure 5 shows typical long time scale temperature and temperature gradient data where the temperature was changed by 0.15 °C at time $\tau=0$ s. From Fig. 5(a), one observes that after 3.5 h the system has reached its final equilibrium temperature and is stable to within ~ 0.5 mK over many hours. Figure 5(b) depicts temperature gradient data

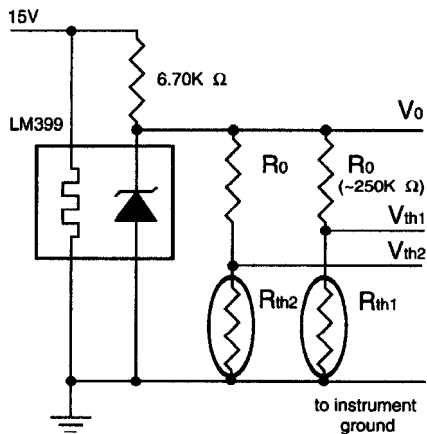


FIG. 4. Series circuit for accurately measuring temperatures and temperature gradients. The thermistor resistances (R_{th1} , R_{th2}) are determined by accurately measuring the voltages V_0 , V_{th1} , and V_{th2} and then converting these resistances to temperatures using the associated thermistor calibration table.

collected using matched thermistors where one observes that the temperature gradient holds steady at less than 0.5 mK/cm over the measurement period.

In our first experimental test of this oven, we have studied the liquid/vapor surface of the nonpolar critical liquid mixture 1,1,2,2-tetrabromoethane+n-dodecane in the one-phase region ($T > T_c$). This mixture possesses both good x-ray and ellipsometric contrast. The ellipsometric results were collected with the glass slide and glass support removed from the glass trough (to minimize any optical inter-

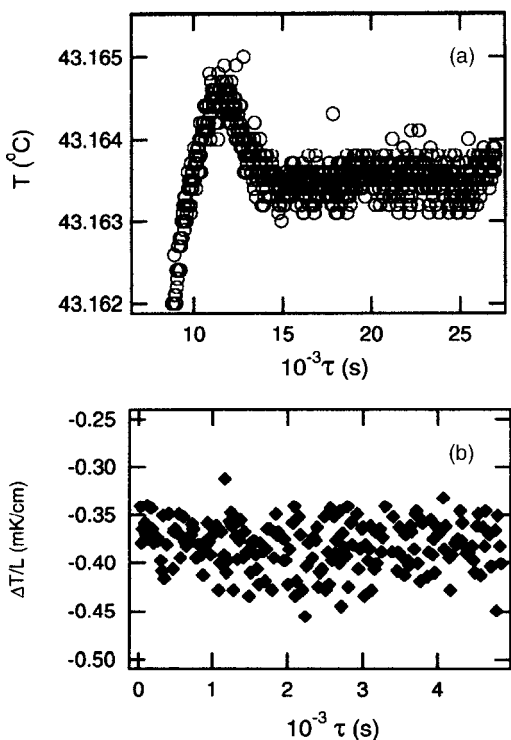


FIG. 5. (a) Variation in temperature after a temperature jump of 0.15 °C at time $\tau=0$ s. The oven has reached its final equilibrium temperature after 3.5 h and is stable to ~ 0.5 mK over many hours. (b) Representative temperature gradient data measured using matched thermistors at either end of the sample cell.

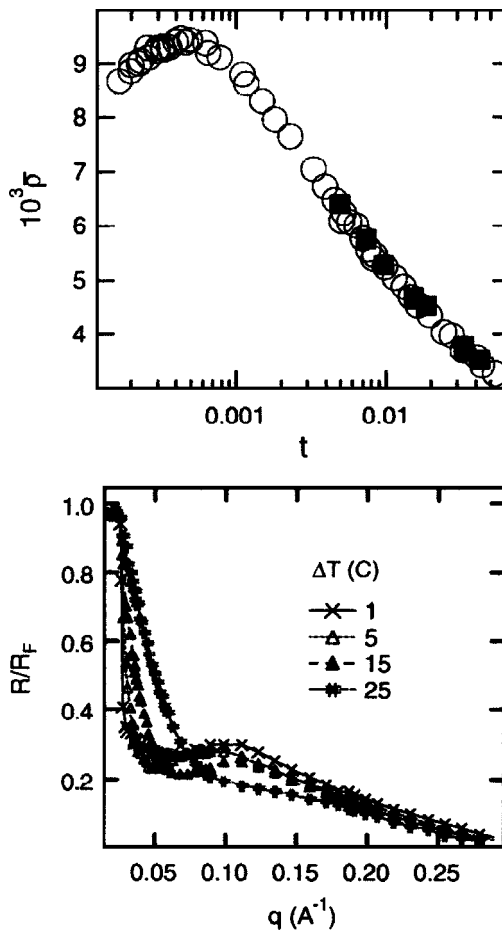


FIG. 6. Experimental measurements from the liquid/vapor surface of the critical mixture 1,1,2,2-tetrabromoethane+n-dodecane. (a) Ellipticity \bar{p} versus reduced temperature t where the current measurements (solid squares) are compared with prior measurements (open circles, Ref. 16). (b) Normalized x-ray reflectivity $R(q)/R_F$ versus scattering vector q at various temperature differences $\Delta T = T - T_c$.

ference) where the results [solid squares, Fig. 6(a)] are compared with earlier measurements (open circles, from Ref. 16). Good agreement is found between these two ellipsometric measurements. X-ray reflectivity [Fig. 6(b)] and off-specular measurements (not shown) were also collected from the liquid/vapor surface of this same stock critical mixture using beamline 9-ID (CMC-CAT) at the Advanced Photon Source located at Argonne National Laboratory. A few mL of the critical mixture overfilled the glass trough. At each temperature, the system was equilibrated for approximately 4 h to ensure thermal and diffusive equilibrium where the x-ray data took an additional 2 h to collect. To prevent the slow degradation of this critical mixture by x rays, a few additional mL of the mixture were added at the end of each x-ray run. The ellipsometric and x-ray data in Fig. 6 demonstrate an interesting fact that was not obvious to us before the measurements. For critical adsorption ellipsometry and x-ray reflectometry are most useful in complementary temperature regimes; ellipsometry exhibits the greatest changes in \bar{p} close to T_c for reduced temperatures $t < 10^{-2}$ (i.e., $T - T_c \leq 3$ °C) whereas, by contrast, x-ray reflectometry exhibits the greatest changes far from T_c for 25 °C $\leq T - T_c \leq 5$ °C. [In Fig. 6(b) the $\Delta T = T - T_c = 1$ °C and 5 °C data are almost identi-

cal, whereas there are large differences between the 5, 15, and 25 °C data.] Complementary ellipsometric and x-ray reflectometry measurements from the same sample are therefore extremely useful in trying to deduce a local volume fraction $v(z/\xi)$ which can describe both data sets. A coherent interpretation of these experimental results is still under consideration.

Finally, we should mention an unexpected problem which arose during the x-ray experiment due to the sample cell design. It was found that at higher temperatures gas bubbles were emitted into the liquid sample from the extraction needle (L2) due to differences in air pressure between the needle and the remainder of the sample chamber. This unintentional problem was overcome by equalizing the pressure via an external tube between L1 and L2. We did not notice any temperature stability or temperature gradient problems with this tube in place.

In summary, we have described the construction of an accurate x-ray and ellipsometry oven which is stable to ~ 1 mK/day and possesses transverse temperature gradients of less than 1 mK/cm. This oven is useful for studying the surface of critical liquid mixtures where accurate temperature control is a prerequisite. The oven can also be used to study adsorption at, for example, the Si wafer/gas interface with the insertion of a Si wafer in place of the glass trough. Neutron reflectometry from the surfaces of these systems can also be undertaken within this oven by replacing the kapton windows with fused quartz windows.

ACKNOWLEDGMENTS

This work was supported by DOE under Grant No. DE-FG03-02ER46020 and NSF under Grant No. DMR-0097119. Work at the CMC Beamlines is supported in part by the Office of Basic Energy Sciences of the U.S. Dept. of Energy and by the National Science Foundation Division of Materials Research. Use of the Advanced Photon Source is supported by the Office of Basic Energy Sciences of the U.S. Department of Energy under Contract No. W-31-109-Eng-38.

- ¹A. W. Adamson, *Physical Chemistry of Surfaces*, 4th ed. (Wiley, New York, 1982).
- ²*Fluid Interfacial Phenomena*, edited by C. A. Croxton (Wiley, New York, 1986).
- ³P. S. Pershan and J. Als-Nielsen, *Phys. Rev. Lett.* **52**, 759 (1984).
- ⁴M. Tolan, *X-ray Scattering from Soft-matter Thin Films*, Springer Tracts in Modern Physics 148 (Springer, Berlin, 1999).
- ⁵R. M. A. Azzam and N. M. Bashara, *Ellipsometry and Polarized Light* (Elsevier, Amsterdam, 1987).
- ⁶See D. Beaglehole in Ref. 2.
- ⁷B. M. Law, *Prog. Surf. Sci.* **66**, 159 (2001).
- ⁸D. Beaglehole, *Physica B & C* **100**, 163 (1980).
- ⁹P. Drude, *The Theory of Optics* (Dover, New York, 1959).
- ¹⁰M. Born and E. Wolf, *Principles of Optics*, 6th ed. (Pergamon, Oxford, 1980).
- ¹¹B. M. Law and D. Beaglehole, *J. Phys. D* **14**, 115 (1981).
- ¹²R. F. Kayser, *Phys. Rev. B* **34**, 3254 (1986).
- ¹³J. L. Tveekrem and D. T. Jacobs, *Phys. Rev. A* **27**, 2773 (1983).
- ¹⁴It should be noted that after the x-ray experiment the chemically resistant Kalrez O-rings had swollen considerably and perhaps teflon-encapsulated O-rings would be a better choice in future.
- ¹⁵*Linear Applications Handbook* (National Semiconductor, Santa Clara, 1986).
- ¹⁶J.-H. J. Cho, B. M. Law, and K. Gray, *J. Chem. Phys.* **116**, 3058 (2002).